Reconfigurable Temporal Fourier Transformation and Temporal Imaging

Zhao Wu, Lei Lei, Jianji Dong, Jie Hou, and Xinliang Zhang, *Member, IEEE*

***Abstract*—We present a multifunctional scheme to implement reconfigurable temporal Fourier transformation (TFT) and temporal imaging (TI) flexibly. This structure is composed of a time lens followed by a section of dispersive fiber with proper length. More specifically, the output waveforms presenting either the spectrum profile or the scaled waveform profile of the input signal are achieved by simply changing the length of the fiber, which is theoretically analyzed and experimentally verified. This proposal requires neither the use of an input dispersive device preceding the time lens nor a second time lens after the dispersion. Hence, it is a simple and practical alternative to the implementation of both TFT and TI.**

***Index Terms*—Dispersive Fourier transformation, fourier optics and signal processing, four wave mixing (FWM), optics fiber communications, time lens.**

I. Introduction

MANIPULATING light in the spatial domain has been proven to be a highly effective approach to perform many types of information processing functionalities, giving rise to the field of Fourier optics [1]. Remarkably, by using the concept known as space-time duality, it is possible to apply these spatial domain technique to the temporal domain, achieving the equivalent functionalities and phenomena in the time domain [2]–[7].

Most notably, the concept of temporal Fourier transformation (TFT) and temporal imaging (TI), originated from the duality of the dispersive propagation performing the role of diffraction while the quadratic phase modulation acting as a time lens [2]–[4], arouses great interest and extensive research. Specifically, TFT is a mapping technique that implements the conversion between the temporal and spectral profile of an input signal [8]–[11], while TI is a waveform manipulation technique that enables compressing or stretching an input waveform while preserving its overall profile [12]–[14]. These techniques enable powerful approaches to sophisticated temporal processing and characterization of information, including optical time division multiplexing to wavelength division multiplexing conversion using time domain optical Fourier transformation [8], [9], ultrahigh-resolution waveform measurement based on time-to-frequency mapping [10], [15], real-time spectrum observation utilizing dispersive Fourier transformation [11], [16], and the temporal magnifier employing the TI system [12], [14], [17], etc. However, among these applications, the configurations solely implement the TFT or the TI, but not both of them. As a matter of fact that, the conventional structures for TFT and TI are very similar. Typically, the systems are characterized by two sections of dispersive fibers connected by a time lens. Whereas, it is difficult to alter the structures from one to another or achieve a specific scale ratio of a imaging system, since the input as well as the output dispersions should be changed simultaneously with respect to the quadratic phase shift, i.e., time lens [12], [17].

In several previous reports, the conventional 2-f system and imaging system are simplified to achieve the equivalent functionalities, such as monodirectional mapping between the time and the frequency domains by removing the dispersion device preceding or following a time lens [10], [18]–[22], and TI without the front dispersion [23] which follows the idea of spatial counterpart [24]. After further investigation, we find that it is feasible to implement reconfigurable TFT and TI in a single system configuration comprising a time lens followed by a dispersive device. In this paper, we propose and demonstrate such a multifunctional scheme by simply changing the output dispersion. Theoretical analysis and experimental results verified that the output waveforms present the spectrum profile and the compressed or stretched waveform profiles of the input signal on the dependence of the fiber dispersion. More specifically, with the increase of the output dispersion, the waveform first compresses and then evolves into its spectrum profile, afterwards it transfers back to the waveform profile and stretches gradually.

The rest of this paper is organized as follows. Section II describes the principle of the reconfigurable TFT and TI based on a time-lens followed by a section of dispersive fiber. In addition, the simulated result is presented to verify the operation principle. Section III experimentally demonstrates the reconfigurable TFT and TI. Then Section IV discusses the feasible implementations and possible applications of the scheme in practice, and Section V concludes this paper.

II. Operation Principle

The concept of the reconfigurable TFT and TI relies on the principle of space-time duality, which indicates that a temporal dispersive propagation of a pulse is analogous to the spatial diffractive propagation of a light beam, and a quadratic phase modulation (i.e., time lens) plays the role of a spatial lens. Fig. 1 shows the schematic diagrams of the reconfigurable TFT and TI through comparing with the spatial counterpart. As shown in

Manuscript received May 25, 2014; revised September 2, 2014 and September 29, 2014; accepted September 30, 2014. Date of publication October 1, 2014; date of current version October 20, 2014. This work was supported in part by the National Basic Research Program of China under Grant 2011CB301704, the Nature Science Fund for Distinguished Young Scholars under Grant 61125501, the NSFC Major International Joint Research Project under Grant 61320106016, and the National Natural Science Foundation of China under Grant 60901006.

The authors are with the Wuhan National Laboratory for Optoelectronics, Huazhong University of Science and Technology, Wuhan 430074, China (e-mail: zwu@hust.edu.cn; leilei@hust.edu.cn; jjdong@mail.hust.edu.cn; houjie@hust.edu.cn; xlzhang@mail.hust.edu.cn).

Color versions of one or more of the figures in this paper are available online at http://ieeexplore.ieee.org.

Digital Object Identifier 10.1109/JLT.2014.2361293

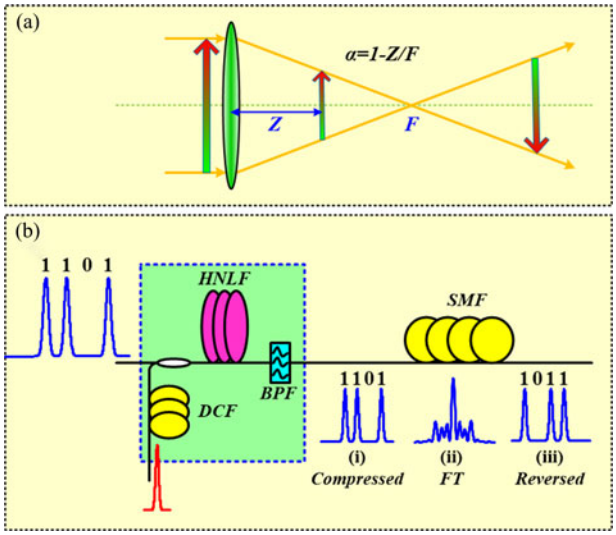

Fig. 1. Schematic diagram of the (a) spatial and (b) temporal system for Fourier transformation and imaging.

Fig. 1(a), an object placed at the near front of a thin lens projects to an image at a distance of Z behind the lens, whose focus length is F. At the back of the lens before its back focus plane, i.e., $\mathrm{Z} < \mathrm{F}$, the upright image shrinks firstly and compresses gradually as the distance Z increases. Then at the back focal plane of the lens, i.e., $\mathrm{Z} = \mathrm{F}$, the light beam focuses on a bright spot. Here, the intensity distribution of the spot shows exactly the Fourier transform profile of the object. Subsequently, next to the focus, i.e., $Z > F$, the reversed profile of the object appears, and it stretches along with the further increase of the distance Z. According to the behavior in geometry-comparability as shown in Fig. 1(a), the scale ratio of the projected image is $\alpha = 1 - Z/F$. More specifically, the image is upright and compressed at the back of the lens within the focus, i.e., $Z < F$ and $0 < \alpha < 1$, while it is reversed beyond the focus, i.e., $Z > F$ and $\alpha < 0$.

Analog to the spatial counterpart, this phenomenon can be realized in the time domain based on the space-time duality. As illustrated in Fig. 1(b), for a pulse stream of "1101" passing through a time lens and then experiencing a section of dispersive fiber, the output signal presents either the scaled waveform or FT of the input signal depending on the length of the dispersive fiber. In this system, the time lens is implemented by using the parametric mixing process of the signal with a linearly chirped pump pulse [8], [9], [12], [25], which is achieved by transmitting a short pulse through a section of dispersive fiber, so that the quadratic phase profile is imparted on the signal. Here, D_f is induced to describe the focal group delay dispersion (GDD) of the time lens [2]. Consequently, a compressed pulse stream of "1101" is firstly obtained when the output dispersion is less than D_f, and it keeps compressing gradually as the output dispersion increases. Subsequently, when the output dispersion is exactly equal to D_f, a short pulse exhibiting the spectrum profile of the input is achieved. Finally, a reversed pulse stream of "1011" is obtained when the output dispersion exceeds D_f, and it stretches with a further increase of the output dispersion. Thus, within this system configuration, a waveform presenting a spectrum profile as well as a scaled and reversed waveform profile of the input signal can be obtained by simply changing the length of the fiber.

The theoretical derivation is presented as follows. For a dispersive fiber with a flat amplitude and quadratic phase over a certain bandwidth, its corresponding impulse response is given by $\exp(-\mathrm{j}t^2/2\Phi_2)$ when neglecting the amplitude coefficient [6], [26], [27], where Φ_2 is the GDD coefficient of the dispersion parameter, that is, $\Phi_2 = \beta_2 \mathrm{L}$, β_2 donates the group velocity dispersion parameter and L is the length of the fiber. Considering a signal $x(t)$ passing through a time lens $\exp(\mathrm{j}t^2/2\mathrm{D}_f)$ and then a dispersive fiber $\exp(-\mathrm{j}t^2/2\Phi_2)$ successively, the output field is expressed as

$$y(t) \propto \left[x(t)\exp\left(j\frac{1}{2D_f}t^2\right)\right] * \exp\left(-j\frac{1}{2\Phi_2}t^2\right) \quad (1)$$

where $*$ denotes the convolution operation, and the symbol $\propto$ indicates that the two functions are proportional. Then the amplitude of the output waveform is modified to

$$|y(t)| \propto \left|\int_{-\infty}^{+\infty} x(\tau)\exp\left[j\left(\frac{1}{2D_f}-\frac{1}{2\Phi_2}\right)\tau^2\right] \exp\left(j\frac{1}{\Phi_2}t\tau\right)d\tau\right|. \quad (2)$$

When the dispersion equals to the focal GDD of the time lens, that is $\Phi_2 = \mathrm{D}_f$, the output is

$$|y(t)| \propto \left|\int_{-\infty}^{+\infty} x(\tau)\exp\left(j\frac{1}{\Phi_2}t\tau\right)d\tau\right|. \quad (3)$$

According to the Fourier transformation characteristics, the output is written as

$$|y(t)| \propto \left|X\left(f=-\frac{t}{2\pi D_f}\right)\right| \quad (4)$$

which represents the spectral profile of the input signal. The scale ratio is related to the GDD of the time lens.

On the other hand, when the dispersion deviates from the focal GDD of the time lens, that is $\Phi_2 \neq \mathrm{D}_f$, the output is modified from Eq. (2) and expressed as

$$|y(t)| \propto \left|\int_{-\infty}^{+\infty} x(\tau)\exp\left[j\left(\frac{1}{2D_f}-\frac{1}{2\Phi_2}\right)\left(\tau-\frac{1}{1-\frac{\Phi_2}{D_f}}t\right)^2\right]d\tau\right|. \quad (5)$$

In this case, if the output dispersion appropriately deviates from the GDD of the time-lens and satisfies

$$\left|\frac{1}{2D_f}-\frac{1}{2\Phi_2}\right| \gg \frac{1}{\Delta T^2} \quad (6)$$

where ΔT is the temporal width of the input signal, then the stationary-phase approximation is applied to simplify the integral [28], [29], resulting in

$$|y(t)| \propto \left|x\left(\frac{t}{1-\Phi_2/D_f}\right)\right|. \quad (7)$$

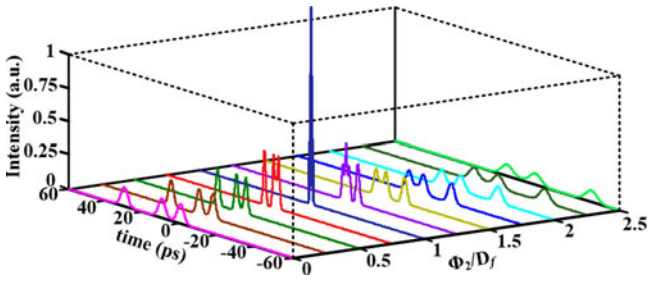

Fig. 2. Evolution of the waveform along with the increase of the fiber length.

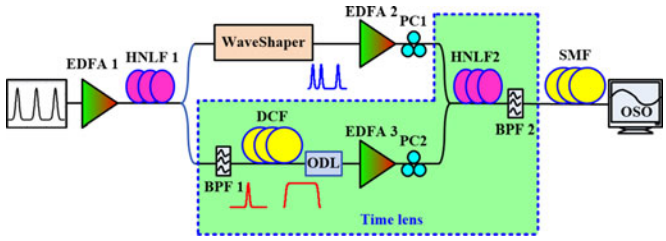

Fig. 3. Experimental setup of the reconfigurable TFT and TI.

Thus, the output waveform is a replica of the input waveform with the scale ratio of

$$\alpha = 1 - \frac{\Phi_2}{D_f} \tag{8}$$

which is in accordance with the spatial counterpart.

Therefore, if the dispersion is less than the focal GDD of the time lens, i.e., $\Phi_2 < \mathrm{D}_f$, the output waveform is a non-reversed and compressed replica of the input waveform, that is $0 < \alpha < 1$. While at the GDD of the time lens, i.e., $\Phi_2 = \mathrm{D}_f$, the waveform resembles the spectrum of the input signal. When the dispersion exceeds the focal GDD of the time lens, i.e., $\Phi_2 > \mathrm{D}_f$, the output waveform shows a reversed and scaled profile of the input waveform, that is $\alpha < 0$. Normally, it is hard to achieve a TI around the GDD of the lens since the imaging condition implied by inequality (6) is not satisfied and the stationary-phase approximation cannot be applied to simplify the integral in Eq. (5). In this case, the projected waveform is considered in a transitional state between the FT profile and the scaled imaging profile of the input signal.

Fig. 2 shows the simulated result presenting the evolution of the waveform with the accumulated dispersion Φ_2 of the fiber. The input signal is a pulse stream of "1101", after passing through a time lens with a GDD of D_f, the waveform compresses along with increasing of the fiber length firstly and then presents the spectrum profile of the input signal at the focal GDD of the time lens. Afterwards, the reversed waveform of the input signal appears and it stretches with further increase of the fiber length, which agrees well with the previous description. Thus in this system, the reconfigurable TFT and TI with different scale ratios are achieved depending upon the output dispersion. Around the focal GDD of the time lens is the transitional zone.

III. Experimental Setup and Results

The experimental setup of the reconfigurable TFT and TI is shown in Fig. 3. An external cavity semiconductor mode-locked pulse source emits a pulse train with a repetition rate of 10 GHz centered at 1548.88 nm and a full-width at half maximum (FWHM) of ~2 ps. The pulse sequence is amplified and spectrally broadened through self-phase modulation, generating a supercontinuum in a 1000 m dispersion-flattened highly nonlinear fiber (HNLF) with nonlinear coefficient of 10/W/km, from which both data and pump spectra are filtered out. In the upper branch, the 10 GHz pulse train for the data signal is obtained via a programmable spectral pulse shaper (Finisar WaveShaper), which acts as a combined filter consisting of a band pass filter (BPF) and a finite impulse response (FIR) filter. The BPF is centered at 1554 nm with a 3 dB bandwidth of 2 nm, while the FIR filter with a transfer function of $[1 + \exp(j2\pi f\tau) + \exp(j2\pi f3\tau)]/3$ encodes the data "1101" on the pulse sequence, where τ is 10 ps. In the lower branch, the pump pulses is spectrally filtered by a BPF (BPF 1) centered at 1548.88 nm with bandwidth of 1.6 nm. It is then dispersed through a section of dispersion compensation fiber (DCF), which is of premeasured length for compensating accurate dispersion of 3 km single mode fiber (SMF). The dispersion parameters of the DCF and SMF in the experiment are -141.09 and 16.75 ps/nm/km, respectively. An optical delay line is used to align the pump pulse and the data signal. The encoded data signal and pump signal are amplified, and then undergo the following polarization controller (PC). PC1 and PC2 are employed to adjust the polarization states of the data signal and pump signal to get the optimal four wave mixing (FWM) efficiency in the following HNLF. Then the data signal and pump signal are combined using a 3 dB coupler and injected into HNLF2. The power of the data signal and pump pulse injected into the HNLF2 are 15.3 and 16.8 dBm, respectively. The HNLF2 is 135 m long with zero dispersion wavelength at 1549 nm and nonlinear coefficient γ of 20/W/km. The stage of the time-lens is performed using the FWM effect of the HNLF2 between the data signal and pump signal, and the quadratic phase modulation is imparted on the generated idler signal [9], [13]. At the output of the HNLF2, a BPF (BPF 2) with bandwidth of 3.2 nm is employed to extract the idler signal, which propagates through a section of SMF subsequently. In the experiment, the length of the SMF is tuned to demonstrate the reconfigurable TFT and TI process. Finally, the signal is received by an Eye-1100C high-speed optical sampling oscilloscope, in which all-optical sampling technology is exploited.

The waveforms of the encoded data signal and the pump signal are illustrated in Fig. 4(a) and (b), respectively. The data signal is a repeating pulse train of "1101", synthesized by a 10 GHz pulse sequence and its delayed replica with delay times of 10 and 30 ps. The time gap between the two pulse packets is 70 ps, and the FWHM of each pulse is 3.1 ps. The pump signal is broadened pulses stream with linear chirp, generated by dispersing a 10 GHz pulse sequence having broad flat-top spectrum. In this case, the dispersion process maps the spectrum profile of the short pulse into the time domain.

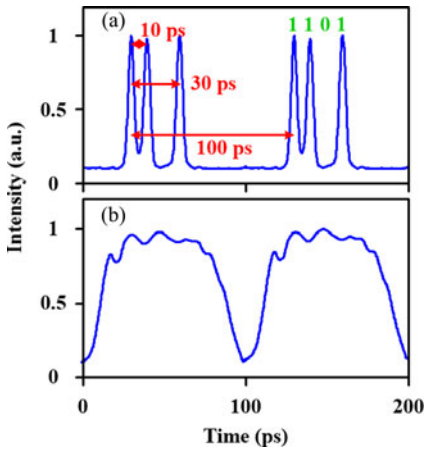

Fig. 4. Waveforms of (a) the encoded data signal and (b) the broadened pump signal.

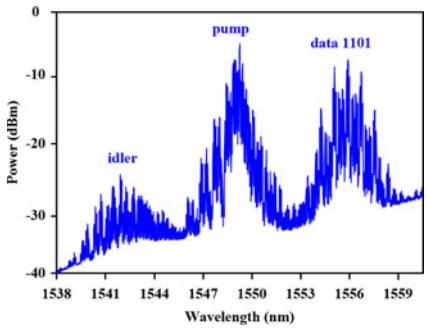

Fig. 5. Spectrum at the output of HNLF2.

The data signal and pump signal are combined and injected into the HNLF2, and the output spectrum of the HNLF2 is illustrated in Fig. 5. The spectrum of the idler signal appears beside the pump signal owing to the FWM process in HNLF2 [30], [31] and is then extracted by a BPF. In this case, the data signal $\mathbf{E}_\mathrm{s}$ is converted to an idler $\eta \mathbf{E}_\mathrm{p}^2 \mathbf{E}_\mathrm{s}{}^*$ combining with the phase of pump signal $\mathbf{E}_\mathrm{p}$, where η is the efficiency factor of the FWM process. On the other hand, due to the degenerate FWM effect, the quadratic phase profile of the pump $\mathbf{E}_\mathrm{p}$ is doubled and imparted on the idler signal, thus the equivalent focal length of the time lens is 1.5 km for the SMF [2], [9].

Afterwards, the idler signal passes through different lengths of SMF and the output waveforms are illustrated in Fig. 6, which show the evolution process of the generated waveform with the gradual increase of the output dispersion, indicating that the reconfigurable TFT and TI can be achieved by simply changing the output dispersion.

Firstly, following the time lens, the waveform is gradually compressed as the fiber length increases. The waveforms at the output of 0.3 and 0.6 km SMFs are illustrated in Fig. 6(a) and (b), respectively. Herein the scale ratios α of the projected images are 4/5 and 3/5 according to Eq. (8). The time intervals of the adjacent pulses are measured to be 8 and 6 ps, respectively, which are in accordance with the theoretical analysis. The non-uniform amplitude of the pulses is partly induced by the non-flat amplitude transmission of the time lens and the dispersion induced phase-to-amplitude conversion [32], [33].

Then at the focal GDD (1.5 km) of the time lens, the waveform resembles the spectrum profile of the signal, as shown in Fig. 6(d). The experimental and simulated results are presented in blue-line and red-dot, respectively. The inset shows an expanded view of the waveforms, showing a good consistency between the experimental and simulated results.

Subsequently, with further increasing of the fiber length, the waveform profile reappears, it is reversed and stretched accordingly. Fig. 6(f)–(h) show the generated waveforms at output of 3, 3.5 and 4 km SMFs, respectively. According to Eq. (8), the scale ratios α of the projected images are -1, $-4/3$, and $-5/3$, respectively. The time intervals of the adjacent pulses are measured to be 10, 14 and 17 ps, which agree well with the expectations. It is noted that, the absolute scale-ratio $|\alpha|$ increases monotonically with the further increase of the output dispersion, and the projected image would overlap with the adjacent one if the dispersion is too large [5]. Thus, in the experiment, the absolute magnification factor is up to 5/3. Larger magnification factor can be achieved by using a lower repetition-rate pulse source, benefiting from the increased time interval between the pulse packets.

Fig. 6(c) and (e) show the output waveforms around the focal GDD of the time lens, indicating that it is difficult to achieve TI nearby the Fourier transformation point of the time lens. In these cases, the output dispersions are provided by 1 and 2 km SMFs, respectively, and the conditions for imaging as implied in Eq. (6) are not satisfied. Fig. 6(c) and (e) show the transitional states between the TFT and TI.

The evolution of the waveform profile along with the fiber length is a transformation process from the waveform profile to the spectrum profile, and then back to the waveform profile of the signal. The waveform profile around the focal GDD is a transitional profile between the spectral profile and waveform profile of the signal. Therefore, the reconfigurable TFT and TI are achieved on the dependence of the output dispersion.

IV. Discussion

In practice, the feasible implementation for the desired reconfigurability of the scheme can be achieved in two ways. The first one is based on the fixed time lens followed by a tunable dispersion device, as illustrated in Fig. 3, where the dispersive fiber is substituted by a tunable dispersion device, such as multistage optical all-pass filter with a micro-electro-mechanical actuated variable reflector and a thermally tuned cavity [34], fiber Bragg grating using beam bending [35], optically pumping [36] or on-fiber integrated heating [37] technique, or prism pair [38], *et al.* Alternatively, the same degree of the reconfigurability can either be achieved based on a tunable time lens combined with a fixed dispersion device. That is to say, the output dispersion is fixed while the GDD of the time lens is variable by tuning the time-lens chirp. In this case, the time-lens is easily reconfigured in other alternative time-lens implementations [2], such as electro-optic modulation in which the phase shift is tuned by the driven voltage of the radio signal [39], [40], or the cross phase

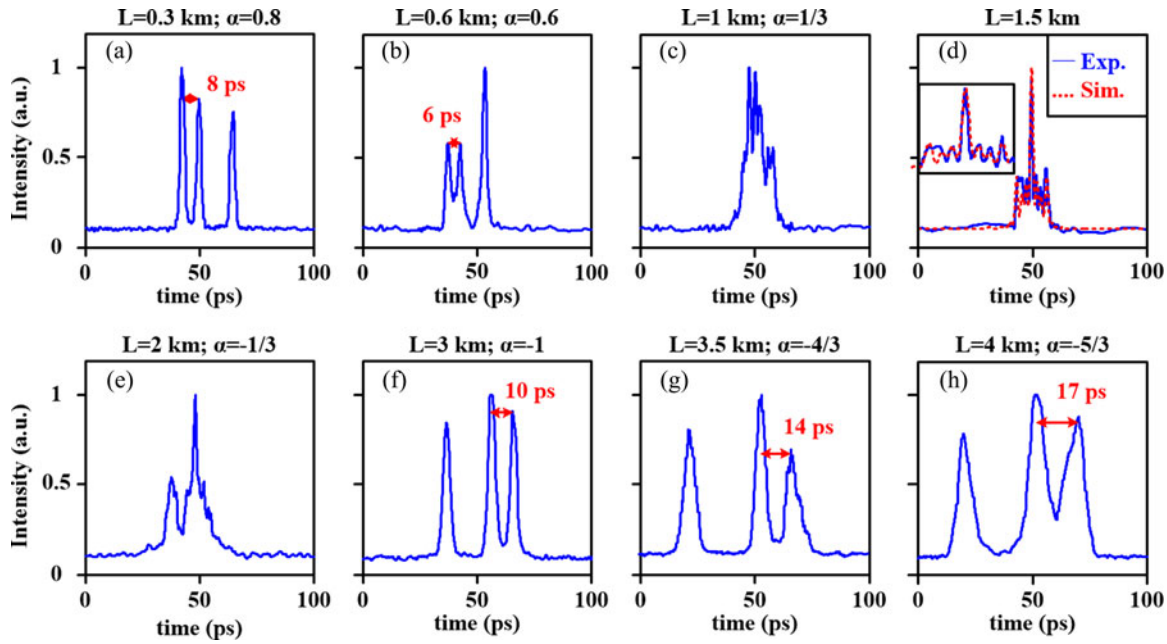

Fig. 6. Waveform at the output of the SMF with length of (a) 0.3 km; (b) 0.6 km; (c) 1 km; (d) 1.5 km; (e) 2 km; (f) 3 km; (g) 3.5 km; (h) 4 km.

modulation via an intensity-dependent refractive index where the phase shift is adjusted through the optical power of the input pump signal [20], [41].

The proposed reconfigurable TFT and TI technique provides a practical alternative to obtain both the real-time spectrum profile and the scaled waveform profile of the input signal flexibly. Thus, it is applicable to acquiring multiaspect information for the evolution of the dynamical processes, especially for nonrepetitive phenomena. On the other hand, by using the TI with scale ratio of -1, the data packet of the transmitted signal gets reversed while preserving its overall scale, showing a great potential for the application of signal encryption and anti-eavesdrop system for secure communication.

V. Conclusion

In this paper, we experimentally demonstrated a scheme for reconfigurable TFT and TI. The system configuration consists of a time lens followed by a dispersive fiber with different lengths. The evolution of the waveform along with the fiber is demonstrated, showing that the temporal Fourier transformed profile and the scaled waveform profile can be achieved within the same configuration by simply altering the fiber length. Moreover, the feasible implementations for the reconfigurability of the proposal are discussed.

References

[1] J. W. Goodman, *Introduction to Fourier optics*, 3rd ed. (Robert, 2005).
[2] R. Salem, M. A. Foster, and A. L. Gaeta, "Application of space-time duality to ultrahigh-speed optical signal processing," *Adv. Opt. Photon.*, vol. 5, no. 3, pp. 274–317, Sep. 2013.
[3] J. V. Howe and C. Xu, "Ultrafast optical signal processing based upon space-time dualities," *J. Lightw. Technol.*, vol. 24, no. 7, pp. 2649–2662, Jul. 2006.
[4] B. Kolner, "Space-time duality and the theory of temporal imaging," *IEEE J. Quantum Electron.*, vol. 30, no. 8, pp. 1951–1963, Aug. 1994.
[5] Z. Wu, J. Dong, J. Hou, S. Yan, Y. Yu, and X. Zhang, "Temporal imaging using a time pinhole," *Opt. Exp.*, vol. 22, no. 7, pp. 8076–8084, Apr. 2014.
[6] Z. Wu, L. Lei, J. Dong, and X. Zhang, "Triangular-shaped pulse generation based on self-convolution of a rectangular-shaped pulse," *Opt. Lett.*, vol. 39, no. 8, pp. 2258–2261, Apr. 2014.
[7] B. Li, M. Li, S. Lou, and J. Azaña, "Linear optical pulse compression based on temporal zone plates," *Opt. Exp.*, vol. 21, no. 14, pp. 16814–16830, Jul. 2013.
[8] K. G. Petrillo and M. A. Foster, "Full 160-Gb/s OTDM to 16 × 10-Gb/s WDM conversion with a single nonlinear interaction," *Opt. Exp.*, vol. 21, no. 1, pp. 508–518, Jan. 2013.
[9] E. Palushani, H. C. Hansen Mulvad, M. Galili, H. Hao, L. K. Oxenlowe, A. T. Clausen, and P. Jeppesen, "OTDM-to-WDM Conversion based on time-to-frequency mapping by time-domain optical Fourier transformation," *IEEE J. Sel. Topics Quantum Electron.*, vol. 18, no. 2, pp. 681–688, Mar. 2012.
[10] M. A. Foster, R. Salem, D. F. Geraghty, A. C. Turner-Foster, M. Lipson, and A. L. Gaeta, "Silicon-chip-based ultrafast optical oscilloscope," *Nature*, vol. 456, no. 7218, pp. 81–84, Nov. 2008.
[11] D. R. Solli, J. Chou, and B. Jalali, "Amplified wavelength-time transformation for real-time spectroscopy," *Nat. Photon.*, vol. 2, no. 1, pp. 48–51, Jan. 2008.
[12] R. Salem, M. A. Foster, A. C. Turner, D. F. Geraghty, M. Lipson, and A. L. Gaeta, "Optical time lens based on four-wave mixing on a silicon chip," *Opt. Lett.*, vol. 33, no. 10, pp. 1047–1049, May 2008.
[13] Y. Okawachi, R. Salem, A. R. Johnson, K. Saha, J. S. Levy, M. Lipson *et al.*, "Asynchronous single-shot characterization of high-repetition-rate ultrafast waveforms using a time-lens-based temporal magnifier," *Opt. Lett.*, vol. 37, no. 23, pp. 4892–4894, Jan. 2012.
[14] V. J. Hernandez, C. V. Bennett, B. D. Moran, A. D. Drobshoff, D. Chang, and C. Langrock, "104 MHz rate single-shot recording with subpicosecond resolution using temporal imaging," *Opt. Exp.*, vol. 21, no. 1, pp. 196–203, Jan. 2013.
[15] A. Pasquazi, Y. Park, S. T. Chu, and B. E. Little, "Time-Lens measurement of subpicosecond optical pulses in CMOS compatible high-index glass waveguides," *IEEE J. Sel. Topics Quantum Electron.*, vol. 18, no. 2, pp. 629–636, Mar. 2012.
[16] K. Goda and B. Jalali, "Dispersive Fourier transformation for fast continuous single-shot measurements," *Nat. Photon.*, vol. 7, no. 2, pp. 102–112, Feb. 2013.

[17] R. Salem, M. A. Foster, A. C. Turner-Foster, D. F. Geraghty, M. Lipson, and A. L. Gaeta, "High-speed optical sampling using a silicon-chip temporal magnifier," *Opt. Exp.*, vol. 17, no. 6, pp. 4324–4329, Mar. 2009.
[18] H. Hu, D. Kong, E. Palushani, M. Galili, H. C. H. Mulvad, and L. K. Oxenløwe, "320 Gb/s Nyquist OTDM received by polarization-insensitive time-domain OFT," *Opt. Exp.*, vol. 22, no. 1, pp. 110–118, Jan. 2014.
[19] F. Li and J. Azaña, "Simplified system configuration for real-time Fourier transformation of optical pulses in amplitude and phase," *Opt. Commun.*, vol. 274, no. 1, pp. 59–65, Jan. 2007.
[20] T. T. Ng, F. Parmigiani, M. Ibsen, Z. Zhaowei, P. Petropoulos, and D. J. Richardson, "Compensation of linear distortions by using XPM with parabolic pulses as a time lens," *IEEE Photon. Technol. Lett.*, vol. 20, no. 13, pp. 1097–1099, Jul. 2008.
[21] M. Nakazawa and T. Hirooka, "Distortion-free optical transmission using time-domain optical Fourier transformation and transform-limited optical pulses," *J. Opt. Soc. Amer. B*, vol. 22, no. 9, pp. 1842–1855, Sep. 2005.
[22] K.-Y. Wang, K. G. Petrillo, M. A. Foster, and A. C. Foster, "Ultralow-power all-optical processing of high-speed data signals in deposited silicon waveguides," *Opt. Exp.*, vol. 20, no. 22, pp. 24600–24606, Oct. 2012.
[23] J. Azana, N. K. Berger, B. Levit, and B. Fischer, "Simplified temporal imaging systems for optical waveforms," *IEEE Photon. Technol. Lett.*, vol. 17, no. 1, pp. 94–96, Jan. 2005.
[24] J. Azaña, J. E. Lugo, A. G. Kirk, and D. V. Plant, "New insights into the problem of shadowlike projection of a plane object illuminated by a spherical wavefront," *Opt. Commun.*, vol. 247, nos. 4–6, pp. 257–264, Mar. 2005.
[25] M. A. Foster, R. Salem, Y. Okawachi, A. C. Turner-Foster, M. Lipson, and A. L. Gaeta, "Ultrafast waveform compression using a time-domain telescope," *Nat. Photon.*, vol. 3, no. 10, pp. 581–585, Oct. 2009.
[26] E. Palushani, L. K. Oxenlowe, M. Galili, H. Mulvad, A. T. Clausen, and P. Jeppesen, "Flat-Top pulse generation by the optical Fourier transform technique for ultrahigh speed signal processing," *IEEE J. Quantum Electron.*, vol. 45, no. 11, pp. 1317–1324, Nov. 2009.
[27] A. Tae-Jung, Y. Park, and J. Azana, "Ultrarapid optical frequency-domain reflectometry based upon dispersion-induced time stretching: principle and applications," *IEEE J. Sel. Topics Quantum Electron.*, vol. 18, no. 1, pp. 148–165, Jan. 2012.
[28] J. R. Klauder, "Path integrals and stationary-phase approximations," *Phys. Rev. D*, vol. 19, no. 8, pp. 2349–2356, Apr. 1979.
[29] J. Rezende, "The method of stationary phase for oscillatory integrals on Hilbert spaces," *Commun. Math. Phys.*, vol. 101, no. 2, pp. 187–206, Jun. 1985.
[30] G. Agrawal, "Nonlinear Fiber Optics," in *Nonlinear Science at the Dawn of the 21st Century*, New York, NY, USA: Springer, 2000, pp. 195–211.
[31] A. E. Willner, S. Khaleghi, M. R. Chitgarha, and O. F. Yilmaz, "All-Optical signal processing," *J. Lightw. Technol.*, vol. 32, no. 4, pp. 660–680, Feb. 2014.
[32] S. Yamamoto, N. Edagawa, H. Taga, Y. Yoshida, and H. Wakabayashi, "Analysis of laser phase noise to intensity noise conversion by chromatic dispersion in intensity modulation and direct detection optical-fiber transmission," *J. Lightw. Technol.*, vol. 8, no. 11, pp. 1716–1722, Nov. 1990.
[33] A. R. Charaplyvy, R. W. Tkach, L. L. Buhl, and R. C. Alferness, "Phase modulation to amplitude modulation conversion of CW laser light in optical fibres," *Electron. Lett.*, vol. 22, no. 8, pp. 409–411, Apr. 1986.
[34] C. K. Madsen, J. A. Walker, J. E. Ford, K. W. Goossen, T. N. Nielsen, and G. Lenz, "A tunable dispersion compensating MEMS all-pass filter," *IEEE Photon. Technol. Lett.*, vol. 12, no. 6, pp. 651–653, Jun. 2000.
[35] T. Imai, T. Komukai, and M. Nakazawa, "Dispersion tuning of a linearly chirped fiber Bragg grating without a center wavelength shift by applying a strain gradient," *IEEE Photon. Technol. Lett.*, vol. 10, no. 6, pp. 845–847, Jun. 1998.
[36] H. Shahoei and J. Yao, "Continuously tunable microwave frequency multiplication by optically pumping linearly chirped fiber Bragg gratings in an unbalanced temporal pulse shaping system," *J. Lightw. Technol.*, vol. 30, no. 12, pp. 1954–1959, Jun. 2012.
[37] B. J. Eggleton, A. Ahuja, P. S. Westbrook, J. A. Rogers, P. Kuo, T. N. Nielsen, and B. Mikkelsen, "Integrated tunable fiber gratings for dispersion management in high-bit rate systems," *J. Lightw. Technol.*, vol. 18, no. 10, pp. 1418–1432, Oct. 2000.
[38] G. M. Gehring, H. Shin, R. W. Boyd, C.-M. Kim, and B. S. Ham, "Tunable optical time delay of quantum signals using a prism pair," *Opt. Exp.*, vol. 18, no. 18, pp. 19156–19162, Aug. 2010.
[39] B. H. Kolner, "Active pulse compression using an integrated electro-optic phase modulator," *Appl. Phys. Lett.*, vol. 52, no. 14, pp. 1122–1124, Apr. 1988.
[40] N. K. Berger, B. Levit, S. Atkins, and B. Fischer, "Time-lens-based spectral analysis of optical pulses by electrooptic phase modulation," *Electron. Lett.*, vol. 36, no. 19, pp. 1644–1646, Sep. 2000.
[41] T. Hirooka and M. Nakazawa, "All-Optical 40-GHz time-domain Fourier transformation using XPM with a dark parabolic pulse," *IEEE Photon. Technol. Lett.*, vol. 20, no. 22, pp. 1869–1871, Nov. 2008.

Zhao Wu received the dual B.Sc. degrees in mathematics and optoelectronics from the Huazhong University of Science and Technology, Wuhan, China, in 2010. He is currently working toward the Ph.D. degree in Wuhan National Laboratory for Optoelectronics and the School of Optical and Electronic Information, Huazhong University of Science and Technology.

His current research interests include optical performance monitoring, optical signal processing technologies, high-speed signal computing and manipulation, and space-time duality technology.

Lei Lei received the B.Eng. degree in electronics information engineering from the Chengdu University of Information Technology, Chengdu, China, in 2009. She is currently working toward the Ph.D. degree in optoelectronics engineering at Wuhan National Laboratory for Optoelectronics, Wuhan, China.

Her current research interests include wavelength converters, all-optical logic gates and circuits, optical computing, novel modulation formats, and optical devices.

Jianji Dong received the B.Eng., M.Eng., and D.Eng. degrees in optoelectronics engineering from the Huazhong University of Science and Technology, Wuhan, China, in 2002, 2005, and 2008, respectively.

He is currently a Professor in Wuhan National Laboratory for Optoelectronics, Wuhan. His current research interests include wavelength converters, all-optical logic gates, microwave phonics, and optical devices.

Jie Hou received the B.Sc. degree in optical information science and technology from the Huazhong University of Science and Technology, Wuhan, China, in 2013. He is currently working toward the Ph.D. degree in Wuhan National Laboratory for Optoelectronics.

His current research interests include all-optical signal processing, optical computing and manipulation, differentiation, integration, and logic gates and related devices.

Xinliang Zhang (M'08) received the Ph.D. degree in physical electronics from the Huazhong University of Science and Technology (HUST), Wuhan, China, in 2001.He is currently with Wuhan National Laboratory for Optoelectronics and the School of Optical and Electronic Information, HUST, as a Full Professor. He is the author or coauthor of more than 160 journal and conference papers including more than 90 IEEE/OSA/IET journal papers. His current research interests include all-optical signal processing and related components.